

Manuscript version: Author's Accepted Manuscript

The version presented in WRAP is the author's accepted manuscript and may differ from the published version or Version of Record.

Persistent WRAP URL:

<http://wrap.warwick.ac.uk/109943>

How to cite:

Please refer to published version for the most recent bibliographic citation information. If a published version is known of, the repository item page linked to above, will contain details on accessing it.

Copyright and reuse:

The Warwick Research Archive Portal (WRAP) makes this work by researchers of the University of Warwick available open access under the following conditions.

Copyright © and all moral rights to the version of the paper presented here belong to the individual author(s) and/or other copyright owners. To the extent reasonable and practicable the material made available in WRAP has been checked for eligibility before being made available.

Copies of full items can be used for personal research or study, educational, or not-for-profit purposes without prior permission or charge. Provided that the authors, title and full bibliographic details are credited, a hyperlink and/or URL is given for the original metadata page and the content is not changed in any way.

Publisher's statement:

Please refer to the repository item page, publisher's statement section, for further information.

For more information, please contact the WRAP Team at: wrap@warwick.ac.uk.

1
2
3
4
5
6
7
8
9
10
11
12
13
14
15
16
17
18
19
20
21
22
23
24
25
26
27
28
29
30
31
32
33
34
35
36
37
38
39
40
41
42
43
44
45
46
47
48
49
50
51
52
53
54
55
56
57
58
59
60

Intrinsic Tuning of Poly(styrene-butadiene-styrene) (SBS) Based Self-healing Dielectric Elastomer Actuators with Enhanced Electromechanical Properties

Christopher Ellingford^a, Runan Zhang^b, Alan M. Wemyss^c, Christopher Bower^b, Tony

McNally^a, Łukasz Figiel^a, Chaoying Wan^{a,}*

Christopher Ellingford, Prof. Tony McNally, Dr. Lukasz Figiel, Dr. Chaoying Wan*,

International Institute for Nanocomposites Manufacturing (IINM), WMG, University of

Warwick, CV4 7AL, UK

**Email: chaoying.wan@warwick.ac.uk*

Runan Zhang, Prof. Christopher Bowen

Department of Mechanical Engineering, University of Bath, BA2 2ET, UK

1
2
3
4 Dr. Alan Wemyss
5
6

7 Department of Chemistry, University of Warwick, CV4 7AL, UK
8
9

10
11 Keywords: self-healing, dielectric elastomer, chemical modification, actuation, electrical
12
13
14
15 breakdown recovery
16
17
18

19
20 Abstract
21
22
23

24
25 The electromechanical properties of a thermoplastic styrene-butadiene-styrene (SBS)
26
27
28 dielectric elastomer was intrinsically tuned by chemical grafting with polar organic groups.
29

30
31 Methyl thioglycolate (MG) reacted with the butadiene block via a one-step thiol-ene 'click'
32
33
34
35 reaction under UV at 25°C. The MG grafting ratio reached 98.5 mol% (with respect to the
36
37
38 butadiene alkenes present) within 20 minutes and increased the relative permittivity to
39
40
41
42 11.4 at 10³ Hz, with a low $\tan \delta$. The actuation strain of the MG grafted SBS dielectric
43
44
45 elastomer actuator was ten times larger than the SBS-based actuator, and the actuation
46
47
48 force was four times greater than SBS. The MG grafted SBS demonstrated an ability to
49
50
51
52
53 achieve both mechanical and electrical self-healing. The electrical breakdown strength
54
55
56
57
58
59
60

1
2
3 recovered to 15% of its original value, and the strength and elongation at break recovered
4
5
6
7 by 25% and 21%, respectively, after three days. The self-healing behaviour was
8
9
10 explained by the introduction of polar MG groups that reduce viscous loss and strain
11
12
13 relaxation. The weak CH/ π bonds through the partially charged (δ^+) groups adjacent to
14
15
16 the ester of MG and the δ^- centre of styrene enable polymer chains to reunite and recover
17
18
19 properties. Intrinsic tuning can therefore enhance the electromechanical properties of
20
21
22 dielectric elastomers and provides new actuator materials with self-healing mechanical
23
24
25 and dielectric properties.
26
27
28
29
30
31
32

33 1. Introduction

34
35
36 Smart electroactive polymers are able to change their shape and size under applied
37
38
39 electric fields, and operate through ionic or electronic actuation mechanisms. Dielectric
40
41
42 elastomers are a class of electronically active polymers¹ which typically exhibit strains up
43
44
45 to 400%, fast response times under an applied electric field and can transduce electrical
46
47
48 energy into mechanical energy (actuation) or *vice versa* for energy harvesting
49
50
51 applications.²⁻³
52
53
54
55
56
57
58
59
60

1
2
3 Dielectric elastomers typically exhibit a low permittivity, which limits performance for
4
5
6
7 actuator and energy harvesting applications due to a low maximum theoretical energy
8
9
10 density, given by Eq.1:

$$U_e = 0.5\varepsilon_r\varepsilon_0E_b^2 \quad (1)$$

16
17 where, U_e is the theoretical energy density, ε_r the relative permittivity, ε_0 the permittivity
18
19
20 of free space and E_b the breakdown strength. The high breakdown strength and low
21
22
23 stiffness of dielectric elastomers, in comparison to piezoelectric ceramic materials, are of
24
25
26
27 interest for use in actuation and energy generation applications. An increase of their
28
29
30
31 relative permittivity has the potential to increase performance significantly, as indicated
32
33
34
35 by Eq.1.

36
37
38 Extensive research has focussed on improving the relative permittivity of dielectric
39
40
41 elastomers, either *extrinsically* through the addition of fillers or *intrinsically* through
42
43
44 chemical modification. The extrinsic approach of incorporating ceramic fillers, such as
45
46
47
48 BaTiO₃,⁴⁻⁵ or electrically conducting metallic or carbon based nanomaterials⁶⁻⁷ has the
49
50
51
52 advantage of using materials with a high relative permittivity to increase the effective
53
54
55
56 permittivity of the composites. However, the enhancement in the relative permittivity of
57
58
59
60

1
2
3 such materials is limited by the poor compatibility between the filler surface and the
4
5
6
7 polymer matrix, and is often at the expense of a reduced breakdown strength,^{1, 8} reduced
8
9
10 mechanical properties⁹ and a large dielectric loss⁹ due to interfacial defects.¹⁰
11
12
13

14 Intrinsic chemical modification of dielectric elastomers is achieved through chemically
15
16
17 grafting polar groups to elastomers to increase the atomic polarisation by increasing the
18
19
20 dipole moment across the polymer chain.¹¹⁻¹³ Chemical modification is advantageous
21
22
23 compared to extrinsic modification methods as it can maintain a low dielectric loss and a
24
25
26 high breakdown strength due to the formation of a homogeneous polymer structure. The
27
28
29 deformable nature of the elastomers can also be maintained after modification.¹
30
31
32
33

34 Small polar groups including allyl cyanide,¹⁴ 3-mercaptopropionitrile¹⁵⁻¹⁶ and 2-
35
36
37 (methylsulfonyl)-ethanethiol,¹⁷ and liquid crystal¹⁸⁻¹⁹ have been grafted to various polymer
38
39
40 structures resulting in an increase in their relative permittivity up to 22.7.¹⁷ Grafting
41
42
43 conducting poly(aniline) to poly(urethane) through a copper phthalocyanine ring resulted
44
45
46 in a large increase in relative permittivity to 105.²⁰
47
48
49
50
51

52 To further enhance the electrical breakdown strength, a novel approach is to enable the
53
54
55 elastomer to self-heal either electrically or mechanically, so that the material can sustain
56
57
58
59
60

1
2
3 large numbers of operational cycles under high electric field conditions without
4
5
6
7 experiencing breakdown.^{1, 21-22} Self-healing is normally achieved through non-covalent
8
9
10 interactions such as hydrogen bonding,²³ π - π stacking and interpenetrating polymer
11
12
13 networks.²² One example of a self-healing actuator has used an iron catalyst incorporated
14
15
16 into poly(dimethylsiloxane) to act as the crosslinker. After mechanically damaging the
17
18
19 material with a hole and leaving it for 72 hours to heal, the material showed no electrical
20
21
22 breakdown at the damaged site until the electric field was 188 kV cm^{-1} .²⁴
23
24
25
26
27

28 In this paper, poly(styrene-butadiene-styrene) (SBS) block copolymer (Vector 8505A)
29
30
31 was chemically grafted with methyl thioglycolate (MG) through a thiol-ene click
32
33
34 chemistry. The SBS material was specifically selected for this study due to its high strain
35
36
37 at break (over 800%), high breakdown strength ($\sim 65 \text{ V } \mu\text{m}^{-1}$)²⁵, and ease of processing
38
39
40 where the available alkene groups on the butadiene block can be readily modified via a thiol-ene
41
42
43 click chemistry. The attachment of polar groups has further increased the tensile strain,
44
45
46 reduced the viscous loss, enhanced relative permittivity without increasing the dielectric
47
48
49 loss, which leads to significantly enhanced electromechanical properties and actuation
50
51
52 performance of the modified SBS. In addition, we demonstrate that the modified SBS
53
54
55
56
57
58
59
60

1
2
3 exhibits rapid self-healing behaviour, which provides the potential to increase the lifetime
4
5
6
7 of the material in actuation and energy generation applications and enable the material
8
9
10 to be reused in the event of failure. The self-healing mechanism is analysed from the
11
12
13 perspective of the macromolecular interactions. This work will inspire further research into
14
15
16
17 the area of self-healing dielectric elastomers to develop materials which not only have
18
19
20
21 excellent mechanical and electrical properties, but also excellent cycle lifetimes and
22
23
24 endurance.
25
26
27
28
29
30

31 2. Experimental

32 2.1. Materials

33
34
35
36
37
38 Styrene-butadiene-styrene block copolymer (SBS, Vector 8508A) was purchased from
39
40
41
42 Dexco. Tetrahydrofuran (THF, GPR Reactapur, 99.9%) was purchased from VWR, UK.
43
44
45
46
47
48 Hexane (for HPLC >95%), chloroform-*d* (99.8%), 2,2-dimethoxy-2-phenylacetophenone
49
50
51
52 (DMPA, 99%) and methyl thioglycolate (95%) were purchased from Sigma-Aldrich, UK.
53
54
55
56
57
58
59
60

1
2
3 All chemical were used as received. Carbon black grease was purchased from MG
4
5
6
7 Chemicals, UK to act as a compliant electrode for actuator studies.
8
9
10
11
12

13 14 2.2. Synthesis 15 16

17
18 In a typical synthesis, 10 g SBS was dissolved in 90 g of THF. Following this, 0.2 g of
19
20 DMPA and 46.9 mL (4× molar excess relative to the butadiene block of SBS) of methyl
21
22 thioglycolate (MG) was added to the solution. The solution was then irradiated with UV
23
24 light @ 365 nm with 25% intensity (50 W) using an OmniCure Series 2000 200 W UV
25
26
27 lamp for 5 to 20 minutes. The resulting modified SBS was purified by precipitation in
28
29
30 hexane and dried in a vacuum oven overnight at 60 °C. The mass of the resulting product
31
32
33 was 21.3 g (98.5% grafting). ¹H NMR (400 MHz, CDCl₃): δ = 7.07 (br, 3 H, H_{benzene}), 6.53
34
35 (br, 2 H, H_{benzene}), 5.39 (br, 4 H, -HC=CH- and HC=CH₂), 3.73 (s, 3 H, COOCH₃), 3.23
36
37 (s, 2 H, OOC-CH₂-S), 2.75 (br, 1 H, (CH₂)₂CHS), 2.64 (br, 2 H, H₂CCH₂S), 1.73 (br, 2 H,
38
39 H₂C-CH₂-CH), 1.55 (br, 6 H, (-H₂C)₂CH₂, -HCCH₂CH₂- and (-HC)₂CH₂), 1.43 (br, 2 H, -
40
41 HCCH₂CH₂), 1.26 (br, 1 H, (H₂C)₃CH) ppm. FT-IR (cm⁻¹): 2927, 1729, 1435, 1272, 1128,
42
43
44
45
46
47
48
49
50
51
52
53
54
55
56 1007, 757. The methyl thioglycolate modified SBS with different graft molar ratios is
57
58
59
60

1
2
3 denoted as MGSBS (x%), i.e., MGSBS (53.7%) @5 mins UV, MGSBS (68.3%) @10
4
5
6
7 mins UV and MGSBS (98.5%) @20 mins UV.
8
9

10 11 12 13 14 2.3. Characterisation 15

16
17 SBS and MGSBS were characterised by ^1H NMR, all spectra were recorded using a
18
19
20
21 Bruker Avance III HD 400 MHz spectrometer. Chemical shifts were internally referenced
22
23
24 to TMS using CDCl_3 . Spectra were processed using ACD/NMR processor version 12.01
25
26
27
28 (ACD/Labs). Gel Permeation Chromatography (GPC) was carried out using an Agilent
29
30
31 390-MDS with two PLgel Mixed-C columns and THF with 2% TEA + 0.01% BHT as an
32
33
34
35 eluent and analysed using Agilent GPC/SEC software.
36
37

38
39 Tensile testing was performed using a Shimadzu Autograph AGS-X tester with samples
40
41
42 conforming to ASTM-D638-14 type V. The extension rate was 50 mm min^{-1} (strain rate =
43
44
45 0.1095 s^{-1}) with a 10 kN load cell and tests were carried out at room temperature. Stress
46
47
48
49 relaxation testing was investigated by stretching the tensile specimens to 100%
50
51
52 elongation at 50 mm min^{-1} and holding the samples at constant strain until the stress
53
54
55
56 reached equilibrium. Cyclic stress softening was performed by elongating specimens to
57
58
59
60

1
2
3 100%, 300% and 500% elongation and back to 0% under a controlled extension rate of
4
5
6
7 50 mm min⁻¹ for 5 cycles. Fourier transform infrared spectroscopy (FT-IR) spectra were
8
9
10 collected using a Bruker Tensor 27 at a resolution of 4 cm⁻¹ with 32 scans. Raman Spectra
11
12
13 were recorded using a Renishaw inVia™ Reflex Raman Microscope with a 532 nm diode-
14
15
16 pumped solid-state laser. Solution state UV-Vis spectroscopy was performed using an
17
18
19 Agilent Cary 60 photospectrometer between 200 nm and 800 nm. Samples were
20
21
22 dissolved in DCM to a concentration of 1×10⁻⁵ mol dm⁻³ . Solid-state UV spectroscopy
23
24
25 was performed on compression moulded thin films of 0.5 mm thickness. Dynamic
26
27
28 Mechanical Thermal Analysis (DMTA) was performed on samples 5.0 mm × 5.0 mm ×
29
30
31 2.3 mm in single cantilever mode with a 50 μm amplitude and a frequency of 1 Hz between
32
33
34 -120 °C and 135 °C. Small Angle X-ray Scattering (SAXS) was carried out using a Xenocs
35
36
37 Xeuss 2.0 SAXS system equipped with both a 1-D and 2-D detector. AFM was imaged
38
39
40 using a Bruker Dimension Icon in Peakforce QNM mode with Scanasyst-Air tips using
41
42
43 tapping mode at a scan rate of 0.2 Hz.
44
45
46
47
48
49
50

51
52 Impedance spectroscopy measurements were carried out using a Princeton Applied
53
54
55 Research Parastat MC with a PMC-2000 card and a two-point probe between 10⁰~10⁶
56
57
58
59
60

1
2
3 Hz on thin films of thickness between 100~200 μm that were formed by compression
4
5
6
7 moulding using a Rondol manual hot press at 190 $^{\circ}\text{C}$ and 5 kN of force.
8
9

10 2.4 Dielectric elastomer actuation 11 12 13

14 To demonstrate the actuation function, the MGSBS and SBS films were coated with a
15
16
17 compliant electrode based on a carbon black grease from MG Chemicals to enable the
18
19
20 two types of elastomers to be actuated under driving voltages (in kV). The following
21
22
23 configurations were arranged: (i) Dielectric elastomer actuation in strain: The MGSBS and SBS
24
25
26 were cut into samples of area 30 mm \times 30 mm and pre-strained by 33.33% in planar directions and
27
28
29 clamped onto the rigid frame as shown in Figure S1a. Carbon black grease was applied to form a
30
31
32 circular electrode region of diameter 15 mm from the centre. The actuation was driven by voltages
33
34
35 of 3, 4 and 5 kV, and the pre-strained state and the actuated state of the samples were recorded by
36
37
38 a camera to allow estimation of the voltage-induced planar deformation. To ensure the actuation
39
40
41 reached a steady state, the actuation state was set to be 5 seconds after switching on the high
42
43
44 voltage power supply. (ii) Actuation in force: The MGSBS and the SBS were cut into samples of
45
46
47 area 40 mm \times 40 mm with a rectangular electrode region of area 20 mm \times 20 mm defined prior to
48
49
50 pre-strain. The samples were then pre-strained by 20% in the direction of actuation, fixed to the
51
52
53 test rig on the top and mounted onto a load cell on the bottom as shown in Figure S1b. The load
54
55
56 cell was customized to measure small forces up to 5 N. The high voltages were applied to the
57
58
59 samples in a sequence that lasted 60 seconds, as shown in Figure S1c. The force was measured by
60
the load cell throughout. A high voltage (HV) generator, based on a HV DC-DC converter

1
2
3 (module 15A24 from PPMTM), was used to amplify the input voltage (0-5 V) to the voltage
4
5
6
7 output (0-15 kV). In the second set of experiments, the actual voltage output was also
8
9
10 measured using a built-in channel from the HV module.
11
12
13
14
15
16

17 3. Results and Discussion 18 19 20 21 22

23 3.1. Chemical Modification of SBS 24 25 26 27

28 MGSBS was synthesised *via* a thiol-ene click reaction in air and at room temperature,
29
30
31 the structures were verified *via* ^1H NMR, FT-IR and GPC. MG was kept in a three or four
32
33
34 times molar excess with respect to the butadiene section of SBS, and no gelation was
35
36
37 detected during the reaction as characterised by ^1H NMR.
38
39
40

41
42 ^1H NMR and FT-IR spectra of the resultant MGSBS are given in Figure 1a and b. In
43
44
45 Figure 1a the characteristic CH_2 and CH_3 peaks in ^1H NMR were observed at 3.23 and
46
47
48 3.73 ppm, respectively, which were absent in the ^1H NMR of SBS, as seen in Figure S2.
49
50
51
52 The reduction in the alkene peaks of the butadiene block at 5.39 and 4.98 ppm is apparent
53
54
55 as the grafting ratio increases, indicating that the reaction of methyl thioglycolate and the
56
57
58
59
60

1
2
3 vinyl groups of butadiene had taken place. Furthermore, FT-IR confirmed the presence
4
5
6
7 of a C=O stretch for an ester group at 1729 cm^{-1} and two C-O stretches at 1272 and 1020
8
9
10 cm^{-1} to indicate the successful grafting of methyl thioglycolate onto the SBS backbone.
11
12
13
14 ^1H NMR was used to determine the grafting efficiency of the reaction at different UV
15
16
17 exposure times. Increasing the UV light exposure time from 5 to 20 minutes resulted in
18
19
20 increasing the grafting ratio of MG to SBS from 53.7% up to 98.5%, with respect to the
21
22
23
24 butadiene block.
25
26
27

28 The number average molecular weight ($M_n=86158\text{ g mol}^{-1}$) and polydispersity index
29
30
31 (PDI=1.17) of SBS chains become 79417 g mol^{-1} and 2.57, respectively, after grafting of
32
33
34 98.5% of methyl thioglycolate, indicating the UV initiated reaction caused some polymer
35
36
37 chain scission. An increase in weight average molecular weight (M_w) from 100768 g mol^{-1}
38
39
40
41 to 203883 g mol^{-1} further confirmed the successful grafting of methyl thioglycolate to SBS.
42
43
44
45
46
47
48

49 3.2. Mechanical and electrical properties of methyl thioglycolate modified SBS

50
51

52 The equations of state for an ideal dielectric elastomer actuator can be expressed in
53
54
55

56 Eq.2,²⁶
57
58
59
60

$$\begin{aligned}\sigma_1 + \varepsilon E^2 &= \lambda_1 \frac{\partial W(\lambda_1, \lambda_2)}{\partial \lambda_1} \\ \sigma_2 + \varepsilon E^2 &= \lambda_2 \frac{\partial W(\lambda_1, \lambda_2)}{\partial \lambda_2}\end{aligned}\quad (2)$$

where, $\sigma_{1,2}$ are the applied stresses in planar directions, $\lambda_{1,2}$ the stretches due to mechanical in planar directions, ε the permittivity of the dielectric elastomer ($\varepsilon = \varepsilon_r \varepsilon_0$), E the applied electric field and $W(\lambda_1, \lambda_2)$ the Helmholtz free energy density. By comparing the un-actuated ($E = 0$) and actuated states, actuation stresses in planar directions, $\Delta\sigma_{1,2}$, correlate to the Maxwell pressure, εE^2 , as expressed in Eq.3,

$$\Delta\sigma_{1,2} \propto \varepsilon E^2 \quad (3)$$

For a dielectric elastomer actuator with equal bi-axial pre-strains, as in the actuation in strain experiment, the actuation strain in the radial direction and change in area due to actuation, Δs_r and Δs_a , correlate to the Maxwell pressure, εE^2 , and the elasticity modulus of the elastomer, Y , as shown in Eq.4.

$$\begin{aligned}s_r &\propto \varepsilon E^2, \frac{1}{Y} \\ s_a &= s_r^2\end{aligned}\quad (4)$$

This indicates for actuation a high permittivity, high breakdown strength and low elastic modulus are desirable, and the mechanical and electrical properties will now be described.

1
2
3
4 The mechanical properties of SBS and MGSBS are shown in Figure 2. After grafting of
5
6
7 98.5% of methyl thioglycolate, the tensile strength and elongation at break of SBS
8
9
10 decreased from 9.00 MPa and 857%, to 3.13 MPa and 569%, respectively. The Young's
11
12
13 modulus of SBS was significantly reduced from 51.7 MPa to 2.87 MPa, which will benefit
14
15
16 the actuation function of dielectric elastomers, and will be discussed in the following
17
18
19 sections.
20
21
22
23

24 The effects of grafting polar groups on the mechanical behaviour was examined by
25
26
27 stress relaxation and cyclic stress softening experiments. The cyclic stress softening
28
29
30 testing of SBS and MGSBS is shown in Figure 2b and c. In Figure 2b, SBS showed large
31
32
33 viscous losses within the samples after five cycles regardless of whether the sample was
34
35
36 elongated 100%, 300% or 500%. In comparison, Figure 2c shows that for MGSBS
37
38
39 (98.5%) the viscous losses are very low for 100% and 300% elongation and are only
40
41
42 observed in significant quantities for 500% elongation. In fact, increasing the grafting of
43
44
45 methyl thioglycolate results in a reduction in the viscous losses exhibited by the material
46
47
48 at strains of 100% to 500%, as shown in Figure 2d.
49
50
51
52
53
54
55
56
57
58
59
60

1
2
3 The stress-relaxation of SBS and MGSBS were evaluated when subjected to a fixed
4
5
6
7 100% elongation until they reached equilibrium. As shown in Figure 3, MGSBS (98.5%)
8
9
10 reached equilibrium after 10 minutes and the stress only decreased by 22%. This shows
11
12
13 that its stronger intermolecular interactions prevent the polymer chains slipping and thus
14
15
16
17 compensate the effect of reduced chain entanglement observed with MGSBS (53.7%).
18
19
20
21 The reduced relaxation of MGSBS (98.5%) will also be of benefit for actuation to maintain
22
23
24 a constant force or displacement.
25
26
27

28 The electrical properties of SBS and MGSBS were characterised by impedance
29
30 spectroscopy. As shown in Figure 4, the initial unmodified SBS has a relative permittivity
31
32
33 of 2.8, and AC conductivity of $1 \times 10^{-9} \text{ S m}^{-1}$ at 10^3 Hz , showing the highly insulating
34
35
36
37 nature of SBS. The grafting of 98.5 % MG to SBS results in an increase in relative
38
39
40
41 permittivity up to 11.4 at 10^3 Hz , close to that of the piezoelectric poly(vinylidene
42
43
44 fluoride).²⁷ While the electrical $\tan \delta$ remains similar to SBS at 9×10^{-3} for 10^3 Hz (where
45
46
47
48 $\tan \delta = \frac{\text{dielectric loss}}{\text{relative permittivity}}$), as seen in Figure 4b. Furthermore, the phase angle of both SBS
49
50
51
52
53
54
55
56
57
58
59
60

1
2
3 and MGSBS remains at -90° , see Figure S3, demonstrating the insulating nature of both
4
5
6
7 elastomers.
8
9

10 The relative permittivity enhancement of the material is higher than that reported for
11
12
13 chemical modification of SBS using an analogous polar group, thioglycolic acid, which
14
15
16 was 7.2 at 10^3 Hz. Other examples in the literature include grafting 3-
17
18 mercaptopropionitrile and 2-(methylsulfonyl)-ethanethiol to polydimethylsiloxane, which
19
20
21 increased the relative permittivity to 18.4 and 22.7 respectively.^{15, 17} However, these
22
23
24 elastomers had dielectric losses several orders of magnitude higher than reported in this
25
26
27 work, reducing their energy transduction efficiency.
28
29
30
31
32
33

34 In summary, the grafting of MG group of 98% to SBS reduced the Young's modulus by
35
36
37 94%, reduced the viscous loss by up to 80% at 300% elongation, while enhancing the
38
39
40 relative permittivity from 2.8 to 11.4, without increasing the dielectric loss. These results
41
42
43 have confirmed the MGSBS as a novel dielectric actuation material, and this is now
44
45
46 demonstrated by evaluation of SBS and MGSBS based actuators.
47
48
49
50
51
52
53
54
55

56 3.3. Dielectric elastomer actuation of SBS and MGSBS 57 58 59 60

1
2
3
4 Figure 5 shows that the MGSBS-based dielectric elastomer actuator generates 10 times
5
6
7 larger actuation strain than the SBS-based DEA. The actuation strain was evaluated
8
9
10 between the state with no electric field and the steady state after 5 seconds of applied
11
12
13 electric field. Under an electric field of 250 kV cm^{-1} , the actuation strain caused MGSBS
14
15
16 radius to increase 13% and the area of MGSBS to increase 17% compared to no
17
18
19 application of electric field. The actuation strain of the SBS under the same electric field
20
21
22 could not be obtained because electrical breakdown occurred in the electrode region
23
24
25 immediately after the application voltage. Instead, the actuation strain of SBS was
26
27
28 recorded at the lower field of 200 kV cm^{-1} . The actuation of SBS increased the radius only
29
30
31
32 1.2% and increased the area 1.4%. Three reasons for the outstanding actuation
33
34
35 performance of the MGSBS compared with the SBS are:
36
37
38
39

40
41 (i) its lower elastic modulus results in larger material deformation under the same Maxwell
42
43 pressure, as discussed in section 3.2, Figure 2.

44
45 (ii) its higher relative permittivity (11.4) that generates larger Maxwell pressure under the same
46
47 driving voltage (i.e. larger s_r and s_a according to Eq.4), as discussed in section 3.2, Figure 4.

48
49 (iii) its higher dielectric strength that allows higher driving voltage (i.e. larger σ_1 , s_r and s_a
50
51 according to Eq.3 and 4).
52
53
54
55
56
57
58
59
60

1
2
3
4 Figure 5 shows the experimental results for dielectric elastomer actuation in force.
5
6
7 Constant voltages were applied on the MGSBS-based and SBS-based actuators for 5
8
9
10 seconds from 3 kV (150 kV cm^{-1}) to 8 kV (400 kV cm^{-1}). Unlike the previous experiments,
11
12
13 no electrical breakdown occurred for both materials since samples are pre-strained to a
14
15
16 lower degree (20% in one direction compared with the equal-biaxial pre-strain of 33% in
17
18
19 two directions), and are therefore thicker and have higher breakdown voltages. In this
20
21
22 experiment, actuation force was defined as the net force between the un-actuated state
23
24
25 and the actuated state (5 seconds after voltage application). For an applied electric field
26
27
28 of 400 kV cm^{-1} , the MGSBS generates an actuation force of 0.12 N, which is four times
29
30
31 higher than the actuation force from the SBS (0.03 N). Unlike the measured the actuation
32
33
34 strain, the actuation force is independent of the elastic modulus of the material and
35
36
37 depends only on the Maxwell pressure (i.e. the relative permittivity of the material). The
38
39
40 difference in actuation forces between the MGSBS and the SBS therefore, according to
41
42
43 Eq.3, agrees well with the results of the improvement in dielectric properties, as in Figure
44
45
46
47
48
49
50
51
52 4.
53
54
55
56
57
58
59
60

3.4 Self-healing of methyl thioglycolate modified SBS

3.4.1 Self-healing after mechanical breakdown

The MGSBS with a grafting ratio of 98.5% exhibited an unexpected, yet remarkable, ability to rapidly recover some of its mechanical properties upon re-attaching two pieces of cut polymer; this was achieved simply by pushing two pieces together at room temperature (RT) without using any other external stimulus. This self-healing behaviour was observed for MGSBS at the higher grafting levels of 68.3% and 98.5%, but not for SBS or MGSBS at a lower grafting of 53.7%.

The extent of self-healing recovery for MGSBS (68.3%) and MGSBS (98.5%) was investigated for varying time periods at RT (thermostatically controlled to 20°C) to determine how the tensile strength and elongation at break recovered over time. As shown in Figures S4a and S4b, a maximum tensile strength recovery of 25.4% (0.80 MPa) and an elongation at break recovery of 20.9% (116.6% strain) were reached after three days (4320 minutes). In comparison, the tensile strength recovery and elongation at break recovery was less than 5% for MGSBS (68.3%).

1
2
3
4 The temperature dependency of self-healing was investigated at 37°C for up to three
5
6
7 days. 37 °C was investigated for self-healing at human body temperature, for potential
8
9
10 biological applications. For samples of MGSBS (98.5%) healed at 37°C, the tensile
11
12
13 strength and elongation at break rapidly recovered to similar levels as those healed at
14
15
16 room temperature, Figure S5. However, subsequent time intervals revealed the samples
17
18
19 reached a maximum tensile recovery of 17.0% (0.5 MPa) and elongation at break
20
21
22 recovery of 13.3% (70% strain), demonstrating a highly temperature sensitive response.
23
24
25
26
27
28 This suggests that the self-healing property is a result of weak intermolecular interactions
29
30
31 that can be easily overcome, which provides further scope for developing high self-
32
33
34 healing elastomers.
35
36
37

38
39 Furthermore, the potential reusability of the material through multiple self-healing cycles
40
41
42 was investigated by using the same samples for all self-healing experiments. Figure 6
43
44
45 shows that after multiple self-healing cycles, the samples had a tensile strength recovery
46
47
48 of 17.7% (0.56 MPa) and elongation at break recovery of 18.9% (105% strain) after three
49
50
51 days. This demonstrates that the MGSBS can be self-healed multiple times without a
52
53
54 major degradation of the self-healing ability.
55
56
57
58
59
60

3.4.2 Self-healing under low electric field

While mechanical self-healing is of interest, the potential for healing after electric breakdown is of interest in dielectric elastomers due to the high operating electric fields. Figure 7a compares the AC conductivity, capacitance and phase angle of MGSBS (98.5%), (i) prior to breakdown, (ii) after breakdown, and (iii) 24 hours after breakdown. Prior to breakdown, MGSBS (98.5%) exhibits a low AC conductivity ($< 1 \times 10^{-9} \text{ S m}^{-1}$), and it is frequency independent at low frequencies ($< 1 \text{ kHz}$) and frequency dependent at high frequencies ($> 1 \text{ kHz}$); this is often termed as the Universal Dielectric Response of many insulating materials including polymers.²⁸ Figure 7b shows that the capacitance of MGSBS (98.5%) is frequency independent for the frequency range studied, indicating a capacitive response due to the low conductivity of the material. The capacitive response can be observed in the phase angle, Figure 7c, where the phase angle is -90° above 100 Hz, since in a capacitive material AC current lags AC voltage by 90° . At low frequencies, the phase angle approaches 0° due to the presence of a small conductivity in the material.

1
2
3 MGSBS (98.5%) was then subjected to dielectric breakdown. A high voltage of 8.5 kV
4
5
6
7 (corresponding to 200 kV cm^{-1}) was applied on the electrode region until electrical
8
9
10 breakdown was detected in voltage monitoring channel of high voltage power supply. The
11
12
13 voltage application was then switched off immediately to stop the failure from further
14
15
16 propagation. Electrical breakdown of the material leads to a formation of a pinhole, with
17
18
19 a diameter of approximately $100 \mu\text{m}$. This is from thermal runaway due to localised Joule
20
21
22 heating in the sample. Joule heating increases the electrical conductivity in those
23
24
25 locations, causing further localised heating until breakdown of the material.²⁹
26
27
28
29
30

31 After dielectric breakdown, the frequency dependency properties change significantly
32
33
34 due to the electrical short circuit formed by the pinhole and a conductive path through the
35
36
37 thickness of MGSBS (98.5%); for example, caused by carbon formation during
38
39
40 breakdown. The AC conductivity increased significantly compared to before breakdown,
41
42
43 Figure 7a, and is now frequency independent, typical of a pure conductor. This is also
44
45
46 observed in the phase angle, which is close to 0° across the entire frequency range,
47
48
49 because current and voltage are in phase for a conductor. The capacitance also
50
51
52 increased significantly, which is common in materials dominated by conductivity.³⁰
53
54
55
56
57
58
59
60

1
2
3
4 After a period of 24 hours, the frequency dependency properties are more similar to
5
6
7 MGSBS (98.5%) before breakdown, where the AC conductivity, capacitance and phase
8
9
10 angle indicate a capacitor behaviour of the healed MGSBS at the low electric fields (25 V
11
12
13
14 cm^{-1}).

17 3.4.3 Self-healing under high electric field

20
21 Figure S6 shows the polarisation – electric field response of MGSBS (98.5%) for applied
22
23
24 voltages up to 4 kV across a sample of approximately 400 μm ; which corresponds to an
25
26
27 electric field of 100 kV cm^{-1} . The polarisation – electric field is linear, since the MGSBS
28
29
30 (98.5%) is capacitive and the constant gradient with field indicates that the permittivity is
31
32
33 insensitive to applied electric field. To achieve electrical breakdown, a higher potential
34
35
36 difference was required (~ 8.5 kV), which corresponds to an electric field of 200 kV cm^{-1} .
37
38
39

40
41 After 24 hours, the low field measurements, Figure 7, indicated healing had taken place;
42
43
44 however, it is important to assess the response of healed MGSBS (98.5%) to higher
45
46
47 electric fields which are typical of operation. The healed material after 24 hours could
48
49
50 survive electric fields of 12.5 kV cm^{-1} , which is 6% of the initial breakdown strength. This
51
52
53
54
55 initially modest healing may be the result of the healed material containing electrically
56
57
58
59
60

1
2
3
4
5
6
7
8
9
10
11
12
13
14
15
16
17
18
19
20
21
22
23
24
25
26
27
28
29
30
31
32
33
34
35
36
37
38
39
40
41
42
43
44
45
46
47
48
49
50
51
52
53
54
55
56
57
58
59
60

conductive regions, such as carbon, which can act as an electric field concentration to limit the amount of healing possible. The application of small mechanical compression to the damaged pinhole region enhanced healing and led to an improvement of the maximum applied electric field after 24 hours to 1.25 kV (31 kV cm⁻¹), which is 15% of the original breakdown strength and similar to the mechanical property recovery (10-25%).

3.4.4 Self-healing mechanism of MGSBS upon mechanical or electrical breakdown

To understand the electrical and mechanical self-healing behaviour of MGSBS, the microstructure evolution of the elastomers was considered. Firstly, as characterised by dynamic mechanical thermal analysis (DMTA), there are two steps in the storage modulus for SBS, Figure 8a, corresponding to the two glass transition temperatures (T_g 's) of the two phases –the polybutadiene block and the polystyrene block. Below T_g , the storage modulus for MGSBS (98.5%) is higher than SBS, reflecting a stronger intermolecular interaction among the MGSBS polymer chains than SBS, making the modified elastomer more rigid. For MGSBS (98.5%) there is a single strong peak for the glass transition temperature and several small peaks in the polybutadiene glass transition region due to

1
2
3 the polymer chains that have been affected by chain scission or have a lower grafting of
4
5
6
7 methyl thioglycolate. From the mechanical $\tan \delta$ results in Figure 8b, the T_g 's occur as a
8
9
10 sharp peak at -83 °C for polybutadiene and a broad peak at 97 °C for the polystyrene
11
12
13 block. In comparison, MGSBS (98.5%) has only one strong decrease in the storage
14
15
16 modulus, resulting in a T_g of -22 °C. The single transition temperature implies that the
17
18
19 grafting of methyl thioglycolate groups has made the two polymer phases compatible.
20
21
22

23
24 The macromolecular interaction of MGSBS was further characterised by UV-vis
25
26
27 spectroscopy. Both SBS and MGSBS (98.5%) in the solution state in dichloromethane
28
29
30 (DCM) and in the solid state were compared. In the solution state in DCM shown in Figure
31
32
33
34 S7, clear peaks for the π - π^* transitions from free styrene and π -stacking styrene groups
35
36
37 are clearly visible for both SBS and MGSBS. However, the π - π^* transition for free styrene
38
39
40 blue shifts by 15 nm to 247 nm because of the chemical modification. This implies that
41
42
43 chemical modification with methyl thioglycolate in the butadiene section results in an
44
45
46 interaction with the styrene block of the polymer, at least in the solution state. In the solid-
47
48
49 state UV-vis spectra in Figure 8c, the π - π^* transition for π -stacking styrene had
50
51
52
53 dramatically increased in its relative intensity to the free styrene transition, when
54
55
56
57
58
59
60

1
2
3 compared to the spectra recorded in the solution state. This peak in MGSBS however
4
5
6
7 was blue-shifted 20 nm compared to SBS. In addition, the free styrene π - π^* transition
8
9
10 peak is also blue-shifted in the solid material from 266 nm to 248 nm. This blue shift
11
12
13 indicates that there is an increase in the transition energy for the styrene groups because
14
15
16
17 of weak hydrogen bonding interactions with the aromatic electron density.³¹ The peak at
18
19
20 205 nm is the transition from the alkenes on the butadiene block, which is not seen after
21
22
23
24 chemical modification.³²
25
26
27

28 Understanding the nature of self-healing was further explored through FT-IR and
29
30
31 Raman spectroscopy. Shifts in the wavenumbers of peaks compared to the starting
32
33
34 materials, or as grafting increases, implies that a change of environment is taking place
35
36
37 and provides an insight into the interactions involved. In both FT-IR and Raman, Figure
38
39
40
41 1b and Figure 8d, the main peak shifts occur through C-O, C=O and C-C bonds on
42
43
44 increasing the grafting concentration of methyl thioglycolate. In FT-IR, a 6 cm^{-1} and 13
45
46
47 cm^{-1} red shift was observed for both C-O bonds on methyl thioglycolate and also a 4 cm^{-1}
48
49
50 red shift for the C=O on the ester. Likewise, a 2 cm^{-1} red shift was also observed for the
51
52
53
54
55
56 C-C aromatic bond of styrene.
57
58
59
60

1
2
3 A 2 cm^{-1} shift is normally attributed to variance in the equipment, however, in this case
4
5
6
7 the same 2 cm^{-1} drop for the C-C aromatic bond is also observed in the Raman spectrum.
8
9
10 This indicates that the C-C bonds have become slightly elongated. Furthermore, the
11
12
13 Raman spectra also show a 4 cm^{-1} red shift for C=O bonds and a 9 and 12 cm^{-1} red shift
14
15
16 for both C-O bonds on methyl thioglycolate. C-H shifts are observed due to grafting of
17
18
19 methyl thioglycolate. Overall, the elongation of the C-C aromatic bonds of styrene and the
20
21
22 ester group of methyl thioglycolate bonds suggest that these are the interacting groups
23
24
25
26 that lead to self-healing. Specifically, self-healing is likely to originate from either the δ^+
27
28
29 CH_2 or δ^+ CH_3 on either side of the ester accepting electron charge from the δ^- centre of
30
31
32 the benzene ring. As the benzene ring is more stabilised, the δ^+ HC-CH aromatic bonds
33
34
35 experience a weaker pull from the centre, hence the slightly longer bond length. Similar
36
37
38 interactions to this are seen in nature that influence the secondary structure of proteins.³³
39
40
41

42
43
44
45 The increased intermolecular interactions and phase compatibility can influence the
46
47
48 polymer morphology evolution. As illustrated by small angle x-ray scattering (SAXS) in
49
50
51 Figure 9a, the 2D SAXS image shows that SBS displays partial long-range order in one
52
53
54 direction before modification. The 1D spectra for SBS also shows strong q peaks at $\sqrt{3}$
55
56
57
58
59
60

1
2
3 and $\sqrt{7}$ and a small hump at $\sqrt{4}$. This demonstrates that SBS has hexagonally arranged
4
5
6 cylindrical styrene microdomains in a butadiene continuous phase.³⁴ In contrast, the 2D
7
8 image of MGSBS clearly shows the solid and homogeneous intensity of the scattering,
9
10
11 indicating a spherical morphology. From the 1D graph, there is a small secondary q-peak
12
13
14 at $\sqrt{3}$ suggesting that the morphology of MGSBS (98.5%) is misaligned spheres rather
15
16
17 than spheres or cylinders due to the lack of q-peaks at $\sqrt{2}$, $\sqrt{4}$ and $\sqrt{7}$.
18
19
20
21
22
23

24 This transition from cylindrical morphology to the more disordered misaligned spherical
25
26 morphology demonstrates a higher degree of mixing of the two polymer blocks or an
27
28 increase in compatibility, which further supports the DMTA results in Figure 8.
29
30
31
32
33

34 The phase morphology of SBS before and after modification to MGSBS were observed
35
36 by AFM and shown in Figure 9b. The SBS phase image shows hard styrene cylinders in
37
38 dark and butadiene phase in light colour, showing a clear phase separation between the
39
40
41 two phases. The height distribution graph for SBS shows two peaks for the two phases,
42
43
44 Figure 9b. In comparison, for MGSBS, the cylindrical styrene phase has disappeared to
45
46
47 show almost one uniform phase. The height distribution graph also shows only a single
48
49
50
51
52
53
54
55
56
57
58
59
60 peak for one phase. The only existence of the styrene phase is the disordered

1
2
3 arrangement of dark dots, small fragments that remain uncompatibilised by the ester. The
4
5
6
7 few styrene spheres remaining give rise to the small q peak at $\sqrt{3}$ in the SAXS 1D graphs.
8
9

10 Therefore, the vast majority of polystyrene block has been compatibilised by the
11
12
13 chemical modification, resulting the two distinct phases with hexagonally arranged
14
15
16
17 polystyrene cylinders in a polybutadiene matrix transforming into a single disordered
18
19
20
21 polymer phase with a small quantity of disordered polystyrene containing spheres.
22
23

24 The above characterisation results indicate that the mechanism of self-healing of
25
26
27 MGSBS is as a result of an interaction between the δ^- styrene ring and the δ^+ groups on
28
29
30
31 either side of the ester of methyl thioglycolate. The transition to a more disordered phase
32
33
34
35 morphology demonstrates the increased compatibility between the two phases to allow
36
37
38
39 some phase mixing. Electrical breakdown of the elastomer occurs when a pinhole is
40
41
42 formed due to the abrupt increase of the local strain and resultant mechanical rupture.¹
43
44

45 ³⁵ In the case of MGSBS, the intermolecular forces between the polymer chains have
46
47
48 reunited the surfaces together to recover the breakdown strength and mechanical
49
50
51
52 properties.
53
54
55
56
57
58
59
60

4. Conclusions

A styrene-butadiene-styrene (SBS) was chemically modified using thiol-ene 'click' chemistry to graft methyl thioglycolate (MG) to the polymer backbone, where a high grafting ratio (98 mol%) of MGSBS were obtained via a one-step method. Detailed characterisation of the materials produced by this new approach provides the first report on the unexpected and remarkable self-healing capability of MGSBS to self-heal electrical and mechanical damage. A tensile strength recovery up to 25.4% and elongation at break recovery of 20.9% after three days was observed. MGSBS (68.3%) and MGSBS (98.5%) could be healed with no external stimuli and was simply performed by pushing two pieces together, yielding an instantaneous healing.

Characterisation indicated that the self-healing ability was caused by CH/ π interactions between the methyl thioglycolate ester and the proton accepting aromatic system of styrene. At a low methyl thioglycolate grafting density, these interactions occurred intramolecularly and had a decreased chain entanglement when compared with SBS, resulting in a lower strength material without self-healing properties. At increased grafting levels, MGSBS displayed a strong self-healing ability and SAXS data indicated a change

1
2
3 in morphology of SBS from hexagonally arranged styrene cylinders to disordered
4
5
6
7 spheres, showing a compatibilisation between the two blocks of SBS.
8
9

10 Grafting of MG group of 98% to SBS has reduced the Young's modulus by 94%,
11
12 reduced the viscous loss by up to 80% at 300% elongation. Impedance spectroscopy
13
14 measurements of MGSBS (98.5%) showed an increase in the relative permittivity of the
15
16 elastomer from 2.8 to 11.4 at 10^3 Hz and maintained a low $\tan \delta$ of 9×10^{-3} . These
17
18 improvements led to improved actuation whereby MGSBS (98.5%) showed superior
19
20 actuation performance compared to SBS, with an increase in area of 17% at an electric
21
22 field of 250 kV cm^{-1} and exhibited an actuation force of 0.12 N upon application of a 400
23
24 kV cm^{-1} electric field, four times greater than SBS. The electrical breakdown for MGSBS
25
26 (98.5%) recovered to 15% of its original breakdown strength after 24 hours of self-healing
27
28 after breaking down at 200 kV cm^{-1} . Overall, this work introduces a new class of self-
29
30 healing dielectric elastomers using interactions typically seen in nature and results in a
31
32 material which not only has excellent mechanical and electrical performances for
33
34 actuation and energy generation applications but an increased longevity of life due to the
35
36 unexpected self-healing nature.
37
38
39
40
41
42
43
44
45
46
47
48
49
50
51
52
53
54
55
56
57
58
59
60

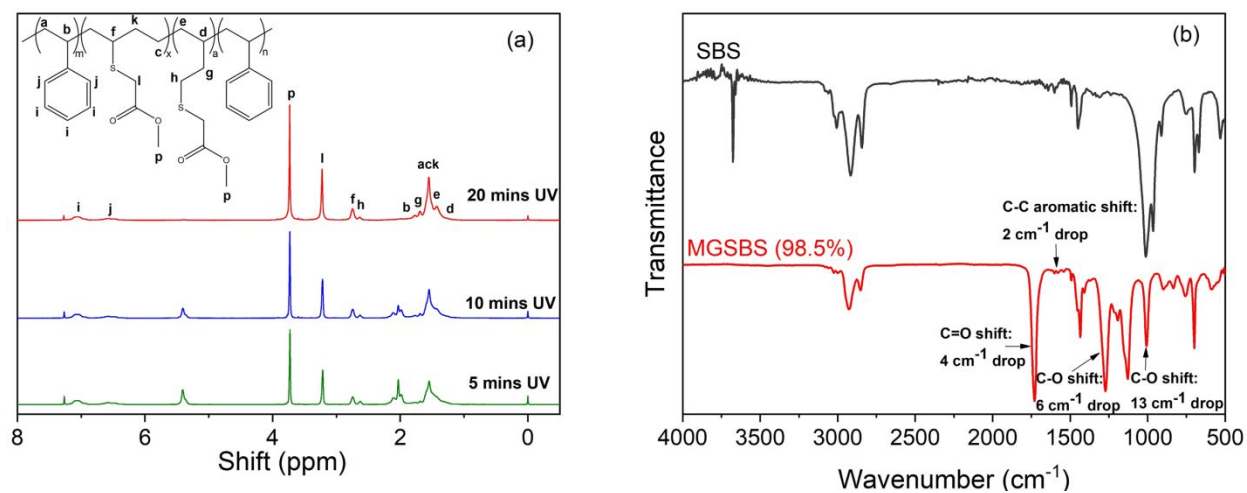


Figure 1. (a) ^1H NMR of MGSBS: grafting 53.7 % @5 mins UV, 68.3 % @ 10 mins UV and 98.5 % @20 mins UV; (b) FT-IR spectra of SBS and MGSBS (98.5%).

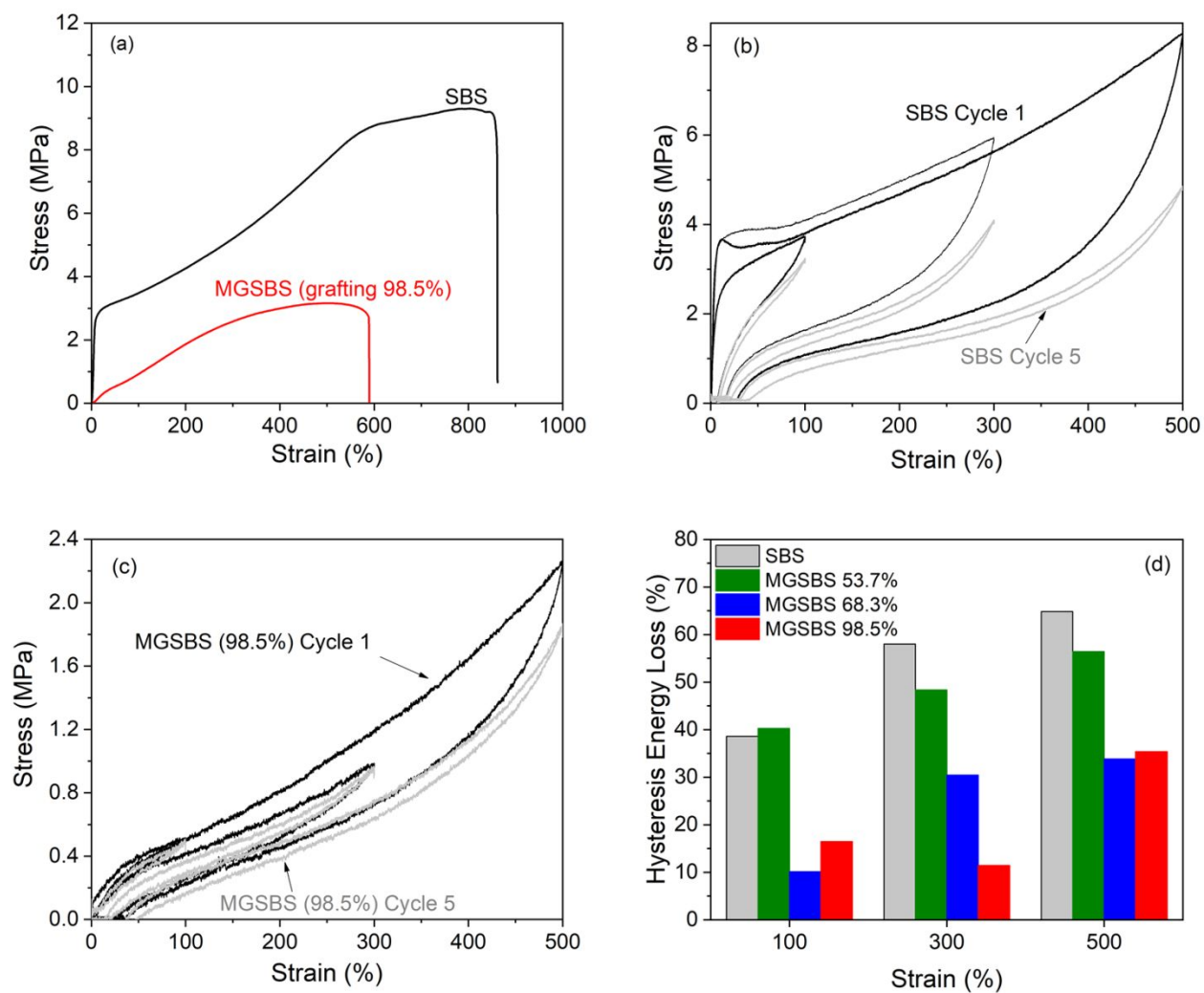


Figure 2. a) Stress-strain curves of SBS and MGSBS (98.5%); b) stress-softening behaviour of SBS at different elongations after 1 cycle and 5 cycles. c) stress-softening behaviour of MGSBS (98.5%) after 1 cycle and after 5 cycles. d) hysteresis energy loss for SBS and MGSBS after 5 cycles.

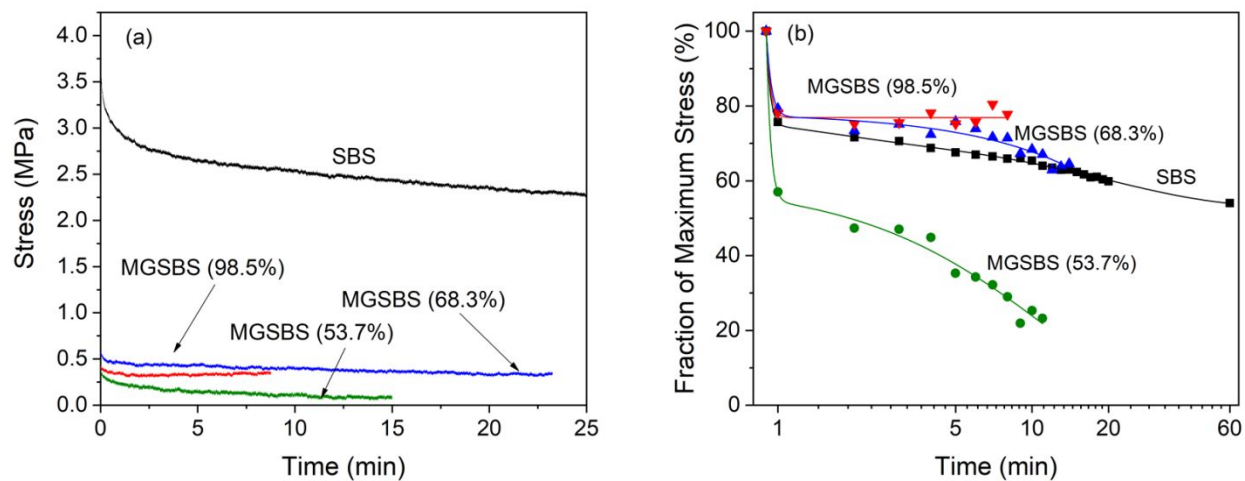


Figure 3. a) Stress vs time curve and b) change in stress compared to initial stress of SBS and MGSBS at grafting ratios of 53.7%, 68.3% and 98.5%

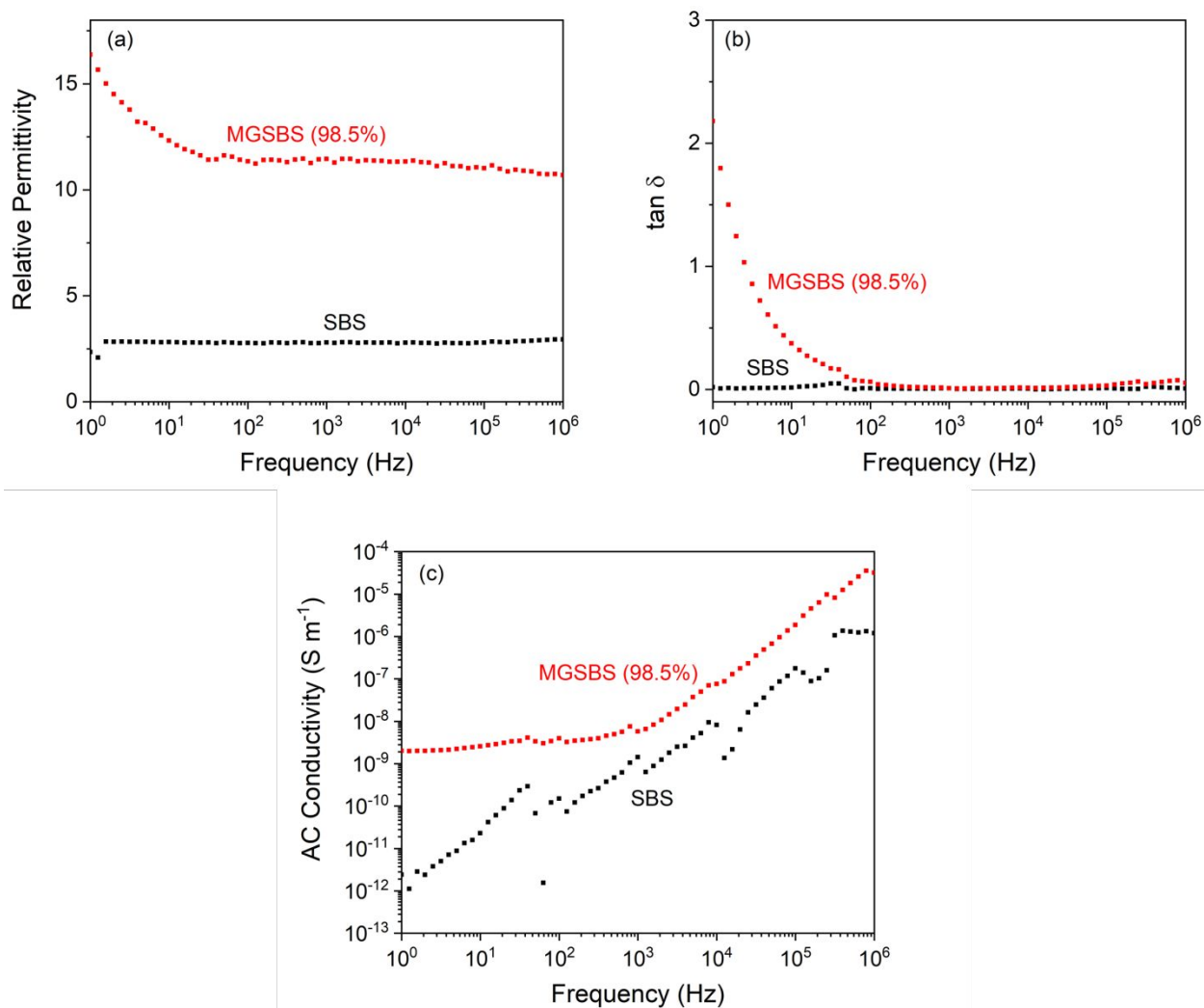


Figure 4. a) Relative permittivity, b) $\tan \delta$, c) AC conductivity of SBS and MGSBS (98.5%).

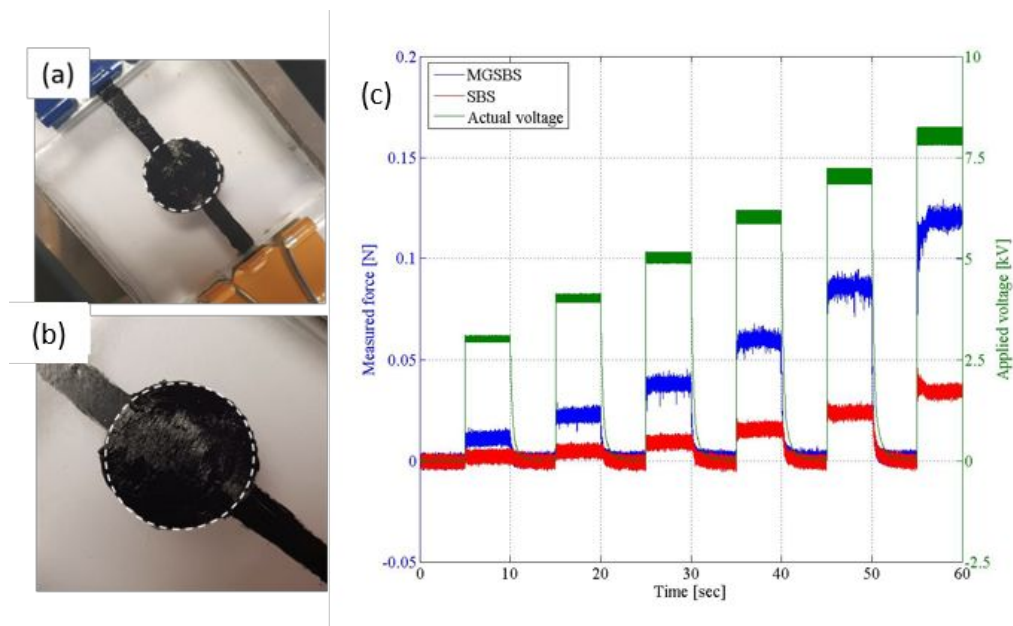


Figure 5. Actuation strain measurement in MGSBS at (a) 0 kV and (b) 5 kV shows the radial strain of approximately 13% and the areal strain of 17%. In comparison, the actuation strain measurement of SBS at 4 kV shows a radial strain of 1.2% and the areal strain of 1.4%. (Electric breakdown occurred immediately after voltage application in SBS at 5 kV; (c) Actuation force measurement in the MGSBS and SBS. At 8 kV, the MGSBS generates 0.12 N while the SBS generates 0.03 N.

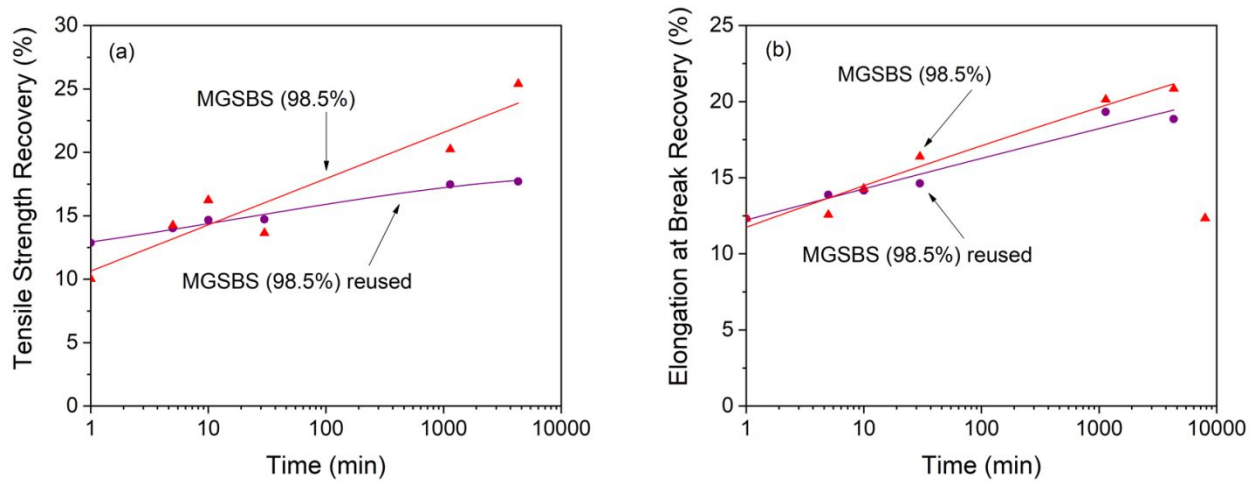


Figure 6. a) Tensile strength recovery; b) elongation at break recovery of MGSBS (98.5%)

native and reused.

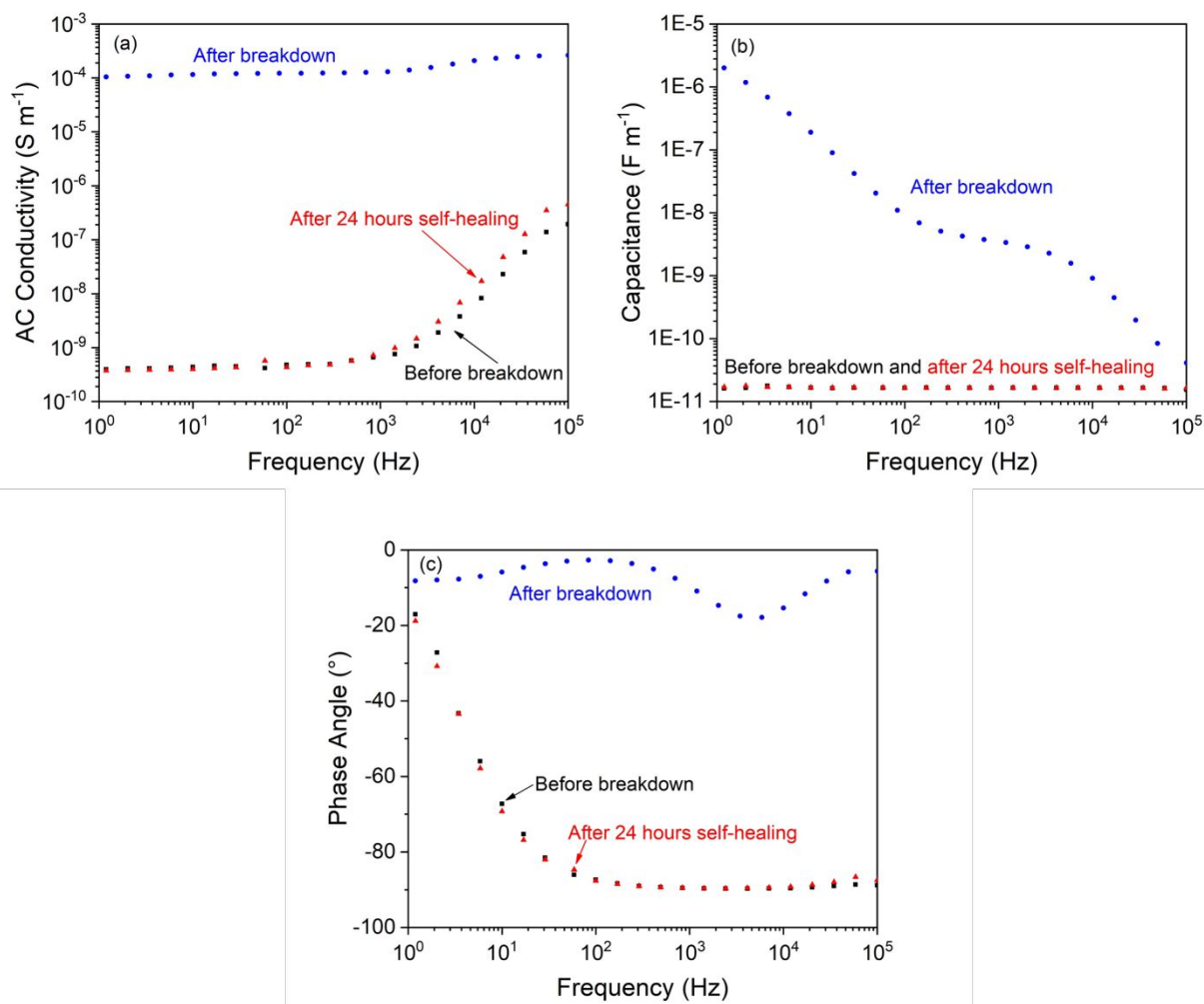


Figure 7. (a) AC conductivity (b) capacitance and (c) phase angle for MGSBS (98.5%)

prior to breakdown, directly after breakdown and 24 hours after breakdown.

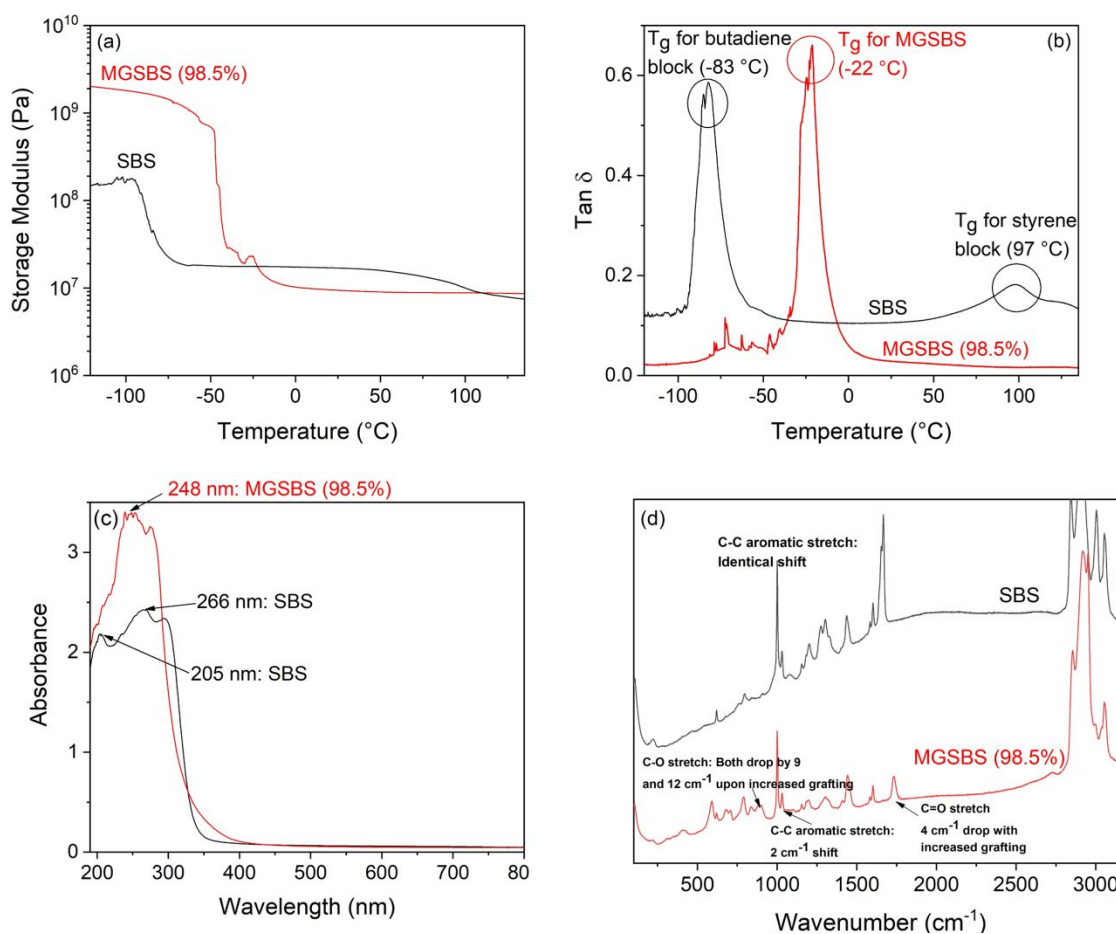


Figure 8. Dynamic mechanical thermal analysis of SBS and MGSBS (98.5%), (a) storage modulus, b) mechanical $\tan \delta$ for the elastomers; c) solid state UV-Vis spectra of SBS and MGSBS (98.5%) and d) Raman spectra of SBS and MGSBS (98.5%).

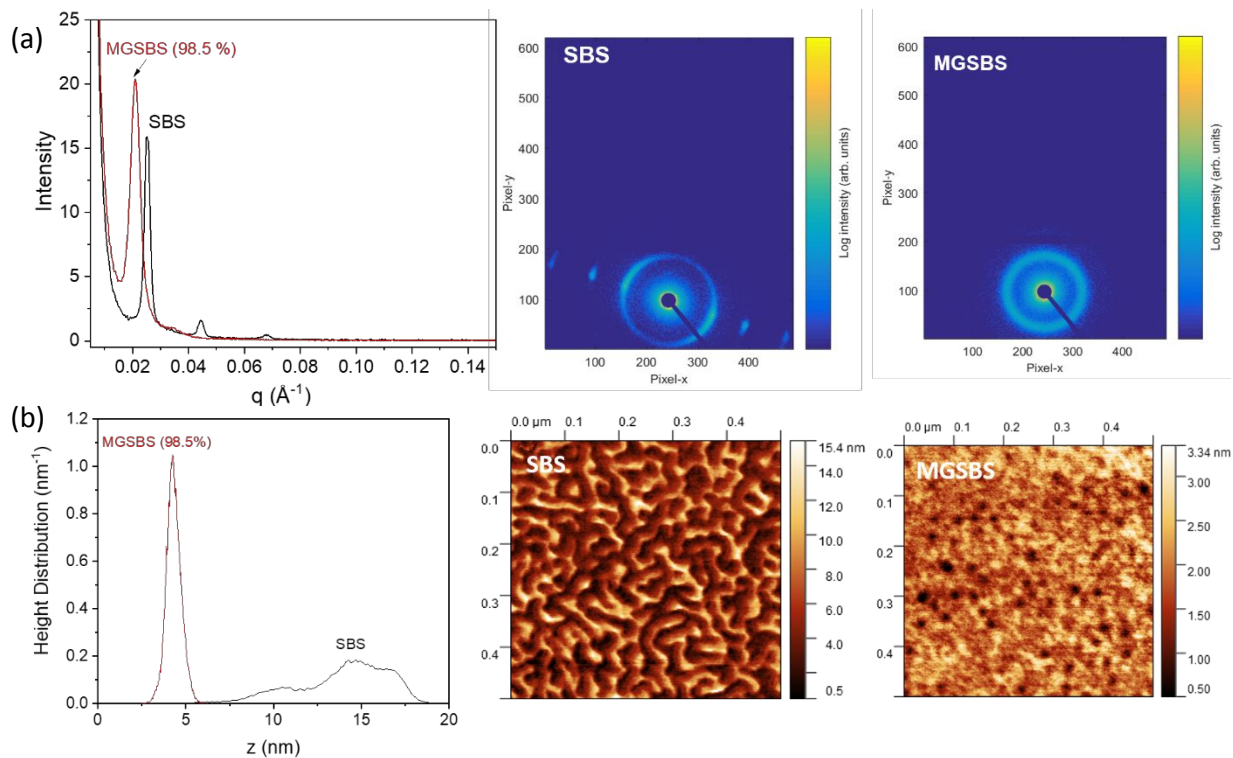


Figure 9. (a) 1D SAXS and 2D SAXS of SBS and MGSBS (98.5%); (b) AFM height distribution and phase morphologies of SBS and MGSBS (98.5%)

ASSOCIATED CONTENT

Supporting Information

- S1: Electrode configurations for (a) dielectric elastomer actuation in strain after pre-strain and setup for actuation strain measurement; (b) dielectric elastomer actuation in force

1
2
3 prior to pre-strain and setup for actuation force measurement; (c) A 60 seconds voltage
4
5 input sequence for actuation in strain.
6

- 7
- 8 • S2: ¹H NMR of SBS.
- 9
- 10 • S3: Phase angle of SBS and MGSBS (98.5%).
- 11
- 12
- 13 • S4: a) tensile strength recovery; b) elongation at break recovery of MGSBS with
14
15 grafting ratios of 68.3 and 98.5%.
16
17
- 18 • S5: a) tensile strength recovery; b) elongation at break recovery of MGSBS (98.5%) self-
19
20 healed at 20 °C and 37 °C.
21
- 22 • S6: Polarisation – electric field response (a) as received material (b) 24 hours after
23
24 breakdown and applied pressure up to 1 kV.
25
- 26 • S7: UV-Vis spectrum of SBS and MGSBS (98.5%) in solution state using DCM.
27
28
29
30
31
32
33
34
35
36
37

38 AUTHOR INFORMATION

41 42 **Corresponding Author**

43
44
45
46 Dr. Chaoying Wan

47
48
49
50 International Institute for Nanocomposites Manufacturing (IINM), WMG, University of
51
52
53
54 Warwick, CV4 7AL, UK
55
56
57
58
59
60

1
2
3 Email: Chaoying.wan@warwick.ac.uk
4
5
6
7
8
9

10 11 12 **Author Contributions**

13
14
15 The manuscript was written through contributions of all authors. All authors have given
16
17
18
19 approval to the final version of the manuscript.
20
21
22

23 **ACKNOWLEDGMENT**

24
25
26
27
28 CE thanks EPSRC and Jaguar Land Rover (UK) for funding this PhD studentship
29
30
31

32 **REFERENCES**

- 33
34
35 (1) Ellingford, C.; Bowen, C.; McNally, T.; Wan, C. Intrinsically Tuning the Electromechanical
36
37 Properties of Elastomeric Dielectrics: A Chemistry Perspective. *Macromol. Rapid Commun.* **2018**,
38
39 *39* (18), 1800340.
40
41
42 (2) Brochu, P.; Pei, Q. Advances in Dielectric Elastomers for Actuators and Artificial Muscles.
43
44 *Macromol. Rapid Commun.* **2010**, *31* (1), 10-36.
45
46
47 (3) Kornbluh, R. D.; Pelrine, R.; Pei, Q.; Heydt, R.; Stanford, S.; Oh, S.; Eckerle, J.,
48
49 Electroelastomers: Applications of Dielectric Elastomer Transducers for Actuation, Generation,
50
51 and Smart Structures. In *SPIE's 9th Annual International Symposium on Smart Structures and*
52
53 *Materials*, SPIE: 2002; Vol. 4698, p 17.
54
55
56
57
58
59
60

- 1
2
3 (4) Yang, D.; Ruan, M.; Huang, S.; Wu, Y.; Li, S.; Wang, H.; Ao, X.; Liang, Y.; Guo, W.; Zhang,
4 L. Dopamine and Silane Functionalized Barium Titanate with Improved Electromechanical
5 Properties for Silicone Dielectric Elastomers. *RSC Adv.* **2016**, *6* (93), 90172-90183.
6
7
8
9
10 (5) Yang, D.; Ge, F.; Tian, M.; Ning, N.; Zhang, L.; Zhao, C.; Ito, K.; Nishi, T.; Wang, H.; Luan,
11 Y. Dielectric Elastomer Actuator with Excellent Electromechanical Performance using Slide-ring
12 Materials/Barium Titanate Composites. *J. Mater. Chem. A* **2015**, *3* (18), 9468-9479.
13
14
15
16
17 (6) Yao, Z.; Song, Z.; Hao, H.; Yu, Z.; Cao, M.; Zhang, S.; Lanagan, M. T.; Liu, H.
18 Homogeneous/Inhomogeneous-Structured Dielectrics and their Energy-Storage Performances.
19 *Adv. Mater.* **2017**, *29* (20), 1601727.
20
21
22
23
24 (7) Dang, Z.-M.; Zheng, M.-S.; Zha, J.-W. 1D/2D Carbon Nanomaterial-Polymer Dielectric
25 Composites with High Permittivity for Power Energy Storage Applications. *Small* **2016**, *12* (13),
26 1688-1701.
27
28
29
30
31 (8) Stoyanov, H.; Mc Carthy, D.; Kollosche, M.; Kofod, G. Dielectric Properties and Electric
32 Breakdown Strength of a Subpercolative Composite of Carbon Black in Thermoplastic Copolymer.
33 *Appl. Phys. Lett.* **2009**, *94* (23), 232905.
34
35
36
37
38 (9) Zhao, H.; Xia, Y.-J.; Dang, Z.-M.; Zha, J.-W.; Hu, G.-H. Composition Dependence of
39 Dielectric Properties, Elastic Modulus, and Electroactivity in (Carbon Black-BaTiO₃)/Silicone
40 Rubber Nanocomposites. *J. Appl. Polym. Sci.* **2013**, *127* (6), 4440-4445.
41
42
43
44
45 (10) Nayak, S.; Chaki, T. K.; Khastgir, D. Development of Flexible Piezoelectric
46 Poly(dimethylsiloxane)-BaTiO₃ Nanocomposites for Electrical Energy Harvesting. *Ind. Eng.*
47 *Chem. Res.* **2014**, *53* (39), 14982-14992.
48
49
50
51
52
53
54
55
56
57
58
59
60

- 1
2
3 (11) Wu, S.; Shao, M.; Burlingame, Q.; Chen, X.; Lin, M.; Xiao, K.; Zhang, Q. M. A High-K
4 Ferroelectric Relaxor Terpolymer as a Gate Dielectric for Organic Thin Film Transistors. *Appl.*
5 *Phys. Lett.* **2013**, *102* (1), 013301.
6
7
8
9
10 (12) Thakur, V. K.; Tan, E. J.; Lin, M.-F.; Lee, P. S. Polystyrene Grafted Polyvinylidene fluoride
11 Copolymers with High Capacitive Performance. *Polym. Chem.* **2011**, *2* (9), 2000-2009.
12
13
14 (13) Putintsev, N. M.; Putintsev, D. N. The Molar Polarization and Refraction of Substances. *Russ.*
15 *J. Phys. Chem.* **2006**, *80* (12), 1949-1952.
16
17
18
19 (14) Racles, C.; Alexandru, M.; Bele, A.; Musteata, V. E.; Cazacu, M.; Opris, D. M. Chemical
20 Modification of Polysiloxanes with Polar Pendant Groups by Co-hydrosilylation. *RSC Adv.* **2014**,
21 *4* (71), 37620-37628.
22
23
24
25 (15) Dunki, S. J.; Tress, M.; Kremer, F.; Ko, S. Y.; Nuesch, F. A.; Varganici, C.-D.; Racles, C.;
26 Opris, D. M. Fine-tuning of the Dielectric Properties of Polysiloxanes by Chemical Modification.
27 *RSC Adv.* **2015**, *5* (62), 50054-50062.
28
29
30
31 (16) Dunki, S. J.; Nuesch, F. A.; Opris, D. M. Elastomers with Tunable Dielectric and
32 Electromechanical Properties. *J. Mater. Chem. C* **2016**, *4* (44), 10545-10553.
33
34
35
36 (17) Dunki, S. J.; Cuervo-Reyes, E.; Opris, D. M. A Facile Synthetic Strategy to Polysiloxanes
37 Containing Sulfonyl Side Groups with High Dielectric Permittivity. *Polym. Chem.* **2017**, *8* (4),
38 715-724.
39
40
41
42
43 (18) Zhang, C.; Wang, D.; He, J.; Liu, M.; Hu, G.-H.; Dang, Z.-M. Synthesis, Nanostructures and
44 Dielectric Properties of Novel Liquid Crystalline Block Copolymers. *Polym. Chem.* **2014**, *5* (7),
45 2513-2520.
46
47
48
49
50
51
52
53
54
55
56
57
58
59
60

- 1
2
3 (19) Zhang, C.; Wang, D.; He, J.; Liang, T.; Hu, G.-H.; Dang, Z.-M. Synthesis and Dielectric
4 Properties of Novel Liquid Crystalline Triblock Copolymers with Cyanobiphenyl Moieties and
5 Poly(n-butyl acrylate) Segments. *Polym. Adv. Technol.* **2014**, *25* (9), 920-926.
6
7
8
9
10 (20) Huang, C.; Zhang, Q. M. Fully Functionalized High-Dielectric-Constant Nanophase
11 Polymers with High Electromechanical Response. *Adv. Mater.* **2005**, *17* (9), 1153-1158.
12
13
14 (21) Dünki, S. J.; Ko, Y. S.; Nüesch, F. A.; Opris, D. M. Self-Repairable, High Permittivity
15 Dielectric Elastomers with Large Actuation Strains at Low Electric Fields. *Adv. Funct. Mater.*
16 **2015**, *25* (16), 2467-2475.
17
18
19
20 (22) Madsen, F. B.; Yu, L.; Skov, A. L. Self-Healing, High-Permittivity Silicone Dielectric
21 Elastomer. *ACS Macro Lett.* **2016**, *5* (11), 1196-1200.
22
23
24
25 (23) Wang, D.; Guo, J.; Zhang, H.; Cheng, B.; Shen, H.; Zhao, N.; Xu, J. Intelligent Rubber with
26 Tailored Properties for Self-healing and Shape Memory. *J. Mater. Chem. A* **2015**, *3* (24), 12864-
27 12872.
28
29
30
31
32 (24) Li, C.-H.; Wang, C.; Keplinger, C.; Zuo, J.-L.; Jin, L.; Sun, Y.; Zheng, P.; Cao, Y.; Lissel, F.;
33 Linder, C.; You, X.-Z.; Bao, Z. A Highly Stretchable Autonomous Self-healing Elastomer. *Nat.*
34 *Chem.* **2016**, *8*, 618.
35
36
37
38 (25) Sun, H.; Jiang, C.; Ning, N.; Zhang, L.; Tian, M.; Yuan, S. Homogeneous Dielectric
39 Elastomers with Dramatically Improved Actuated Strain by Grafting Dipoles onto SBS using
40 Thiol-ene Click Chemistry. *Polym. Chem.* **2016**, *7* (24), 4072-4080.
41
42
43
44 (26) Lu, T.; Huang, J.; Jordi, C.; Kovacs, G.; Huang, R.; Clarke, D. R.; Suo, Z. Dielectric Elastomer
45 Actuators under Equal-biaxial Forces, Uniaxial Forces, and Uniaxial Constraint of Stiff Fibers.
46
47
48
49
50
51
52
53
54
55
56
57
58
59
60

- 1
2
3 (27) Rabuffi, M.; Picci, G. Status Quo and Future Prospects for Metallized Polypropylene Energy
4 Storage Capacitors. *IEEE Trans. Plasma Sci.* **2002**, *30* (5), 1939-1942.
5
6
7 (28) Jonscher, A. K. Low-frequency Dispersion in Carrier-dominated Dielectri. *Philos. Mag. B*
8 **1978**, *38* (6), 587-601.
9
10 (29) Yu, L.; Madsen, F. B.; Skov, A. L. Degradation Patterns of Silicone-based Dielectric
11 Elastomers in Electrical Fields. *Int. J. Smart Nano Mater.* **2017**, 1-16.
12
13 (30) Almond, D. P.; Bowen, C. R. An Explanation of the Photoinduced Giant Dielectric Constant
14 of Lead Halide Perovskite Solar Cells. *J. Phys. Chem. Lett.* **2015**, *6* (9), 1736-1740.
15
16 (31) Sobczyk, L.; Grabowski, S. J.; Krygowski, T. M. Interrelation between H-Bond and Pi-
17 Electron Delocalization. *Chem. Rev.* **2005**, *105* (10), 3513-3560.
18
19 (32) Beavan, S. W.; Phillips, D. Mechanistic Studies on the Photo-oxidation of Commercial
20 Poly(butadiene). *Eur. Polym. J.* **1974**, *10* (7), 593-603.
21
22 (33) Suresh, C. H.; Neetha, M.; Vijayalakshmi, K. P.; Renjumon, G.; Mathew, J. M. Typical
23 Aromatic Noncovalent Interactions in Proteins: A Theoretical Study using Phenylalanine. *J.*
24 *Comput. Chem.* **2009**, *30* (9), 1392-1404.
25
26 (34) Morrison, F. A.; Winter, H. H. The Effect of Unidirectional Shear on the Structure of Triblock
27 Copolymers. I. Polystyrene-polybutadiene-polystyrene. *Macromolecules* **1989**, *22* (9), 3533-3540.
28
29 (35) Moscardo, M.; Zhao, X.; Suo, Z.; Lapusta, Y. On Designing Dielectric Elastomer Actuators.
30 *J. Appl. Phys.* **2008**, *104* (9), 093503.
31
32
33
34
35
36
37
38
39
40
41
42
43
44
45
46
47
48
49
50
51
52
53
54
55
56
57
58
59
60

